

Tunable diode-laser measurement of carbon monoxide concentration and temperature in a laminar methane–air diffusion flame

J. Houston Miller, Salma Elreedy, Bijan Ahvazi, F. Woldu, and P. Hassanzadeh

The application of tunable diode lasers for *in situ* diagnostics in laminar hydrocarbon diffusion flames is demonstrated. By the use of both direct-absorption and wavelength-modulation (second-derivative) techniques, carbon monoxide concentrations and the local flame temperature are determined for a laminar methane–air diffusion flame supported on a Wolfhard–Parker slot burner. In both cases the results are found to be in excellent agreement with prior measurements of these quantities using both probe and optical techniques.

Introduction

Carbon monoxide is an important flame species. A substantial fraction of the heat release in a flame occurs from the CO oxidation reaction: $\text{CO} + \text{OH}\cdot \rightarrow \text{CO}_2 + \text{H}\cdot$. In many combustion systems this reaction is essentially irreversible, which serves as the basis for the development of global oxidation kinetics relationships of the form¹

$$\frac{d[\text{CO}]}{dt} = k_{\text{OV}} \cdot [\text{CO}][\text{O}_2]^{0.25}[\text{H}_2\text{O}]^{0.5}, \quad (1)$$

where k_{OV} represents the effective, overall rate constant for the process. In other combustion systems this reaction is close to equilibration, which may explain the correlation of the CO concentration with the local equivalence ratio (or, alternatively, mixture fraction).²

Because of the effectiveness of its binding with hemoglobin, CO is largely responsible for the loss of life in fire situations.³ In efforts aimed at the development of a predictive capability for CO emissions from fires, various workers have found that CO concentrations can be correlated against overall stoichiometry in the ceiling layers of room fires. Of course, although similar in overall appearance, these correlations are quantitatively different from those

observed within the flame itself.² Because the CO oxidation reaction may effectively be frozen below a certain temperature (because of a decrease in hydroxyl radical concentrations), the conceptual link between in-flame and global correlations will be established through a coupling of a CO oxidation model with a turbulence code capable of predicting the occurrence of this thermal quenching. Although this task may be far into the future, the data required to validate such a model must come from measurements of CO concentrations in both laminar and unsteady diffusion flame conditions. This will eventually require not only quantitative accuracy but also fast temporal response, as can be provided by tunable diode-laser diagnostics.

The emission of soot particles from flames is also likely to affect the concentration of emitted CO. There are two reasons for this. First, large soot particles radiate considerable energy, thus cooling the local flame environment. If the cooling is substantive enough, the rate of CO oxidation will decrease. Second, copious amounts of CO are generated during the oxidative pyrolysis of aromatic compounds.⁴ Because soot essentially has an aromatic structure, CO might be an expected product of the soot oxidation process.

Current measurements of CO concentrations in the flame system used for these studies have been made in two ways: through the use of laser-induced fluorescence technique,⁵ which gives only a relative determination of concentration, and with quartz microprobe–mass spectrometric technique.⁶ In the latter technique profiles of mass spectrometer signal at

The authors are with the Department of Chemistry, The George Washington University, Washington, D.C. 20052.

Received 16 December 1991.

0003-6935/93/306082-08\$06.00/0.

© 1993 Optical Society of America.

molecular weight 28 were collected at three different ionization energies. In this flame there are three species that occur at this mass-to-charge ratio: CO, nitrogen, and ethylene. Because CO has a slightly higher ionization potential than ethylene and a slightly lower one than nitrogen, CO concentrations can be calculated by the subtraction of profiles combined with the application of molecule and ionization-energy specific calibration factors. This is a somewhat cumbersome process and is appropriate only for laminar flames. It should also be noted that this technique is only possible when soot concentrations are quite low because of clogging of the microprobe orifice by particles.^{7,8}

In this paper we will examine the application of tunable diode lasers to the determination of carbon monoxide concentrations and temperature in flames. After describing the experimental configuration, we will demonstrate how simple absorption theory can be applied in diffusion flames and then compare profiles of CO concentration and flame temperature derived from tunable diode-laser measurements with previous experimental determinations.

Experimental Configuration

The tunable diode lasers (TDL's) used in this study are small semiconductor chips composed of a single crystal of a lead salt alloy mounted in a gold-plated copper package. Like all semiconductors, they will conduct electricity when a sufficient voltage is applied. However, these diodes also emit monochromatic, infrared light whose frequency depends on the temperature of the device. With operating temperatures between ≈ 12 and ≈ 60 K, the devices are capable of a spectral output over a range of 50–80 cm^{-1} . (This range is based on our experience. Manufacturer's specifications typically only ensure a diode's performance over 15 cm^{-1} .) Different stoichiometries used in the synthesis of the diodes can be used to produce a spectral emission in the range of 3500–350 cm^{-1} (wavelengths of 2.8–30 μm). In the research described here, a diode with a spectral output between 2090 and 2160 cm^{-1} was used. The diode was mounted in a closed-cycle helium refrigerator, Laser Photonics/Analytics Division (LP/AD) Models 5731 and 5710, which is controlled by a cryogenic temperature stabilizer (Model LP/AD5720). The laser frequency is modulated by adjusting the current through the diodes (current control module Model LP/AD5820); slight modifications of temperature caused by joule heating change the output frequency.

Light emitted from the lasers is not collimated and is rarely single mode. Therefore the beam was collimated with a parabolic mirror, a helium–neon alignment laser beam was superimposed, and the combined beam was directed through a mode-selection monochromator (Model LP/AD5151). The single-mode beam was then steered around the optical mounting table by using reflective optics and was directed into a liquid-nitrogen-cooled InSb detector. The beam could be either electronically modulated or

mechanically chopped. In either case the amplified detector signal was processed through a phase-sensitive, lock-in amplifier (Princeton Applied Research Model 5209). Digitized output from the lock in was recorded on an IBM PC-based data-acquisition system. The overall experimental configuration is shown in Fig. 1.

For wavelength-calibration measurements, spectra of CO and N_2O samples in an ≈ 10 -cm-long absorption cell equipped with NaCl windows were recorded. For the purpose of this assignment, spectral features observed in the cell were generally compared with those recorded in Ref. 10. With these spectral fingerprint data, accurate calibrations of the sine bar of the mode-selection monochromator are possible. In the preparation of gas samples a capacitance manometer was used to determine cell pressure (Leybold–Inficon controller Model CM3 with a Model CM-100 transducer).

In addition to absolute wavelength calibration, it was also necessary to correlate the current through the diode with the relative frequency of the spectral output. Therefore, spectral scans through a germanium etalon with a free spectral range of ≈ 0.048 cm^{-1} were recorded. Current (or, more typically, digital-to-analog converter counts) could be correlated with frequency by using the resulting fringe pattern. Typical spectral scans for CO were over 3000 digital-to-analog counts, which corresponded to a 0.06-A current sweep or ≈ 1.5 cm^{-1} .

The beam waist exiting the monochromator was much too large to be of use as a diagnostic in diffusion flames in which the gradients of temperature and concentration can be quite large.⁶ To reduce the beam size for the flame measurements, we gently focused the beam by using a 500-mm-focal length spherical mirror and recollimated it after the flame with a second, identical mirror. To measure the resulting beam size, we collected a profile of the beam intensity as a razor blade mounted to the burner was swept through the beam. The resulting signal trace represents the integral of the beam intensity pattern in space. If the beam shape is assumed to be Gaussian, then σ , characteristic of the beam size, is calculated to be ≈ 500 μm . This beam size compares favorably with those of other detection techniques that have been applied to diffusion flame structure. In optical experiments using visible or ultraviolet lasers, beam sizes of 50–200 μm were used.^{5,9} For measurements of stable species concentrations using a quartz microprobe–mass spectrometric technique, the sampled volume was estimated to have a diameter of ≈ 700 μm .⁷

For the studies described here, a Wolfhard–Parker slot diffusion burner was constructed from the original shop drawings of the burner used for the last 6 years in our collaborative research with the National Institute of Standards and Technology.^{5–7,9} Air flow was monitored with a Hastings mass flowmeter. Methane flow was metered through a rotameter.

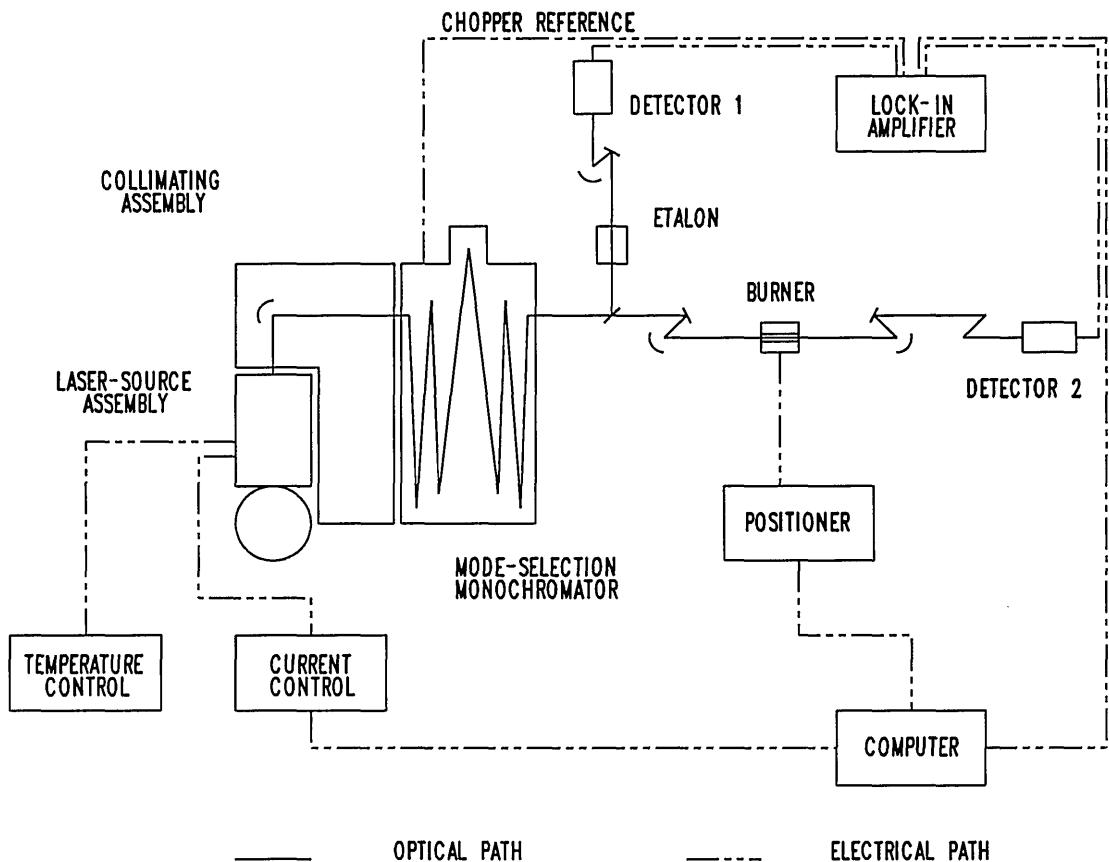


Fig. 1. Experimental configuration for TDL diagnostic measurements in a Wolfhard-Parker slot diffusion flame.

Both flow measuring devices were calibrated against a bubble flowmeter. For most of the experiments the methane fuel rate was $2550 \text{ cm}^3/\text{min}$, which is somewhat higher than that used in prior studies. However, a detailed comparison of profiles collected at flow rates between 1800 and $2800 \text{ cm}^3/\text{min}$ revealed indistinguishable concentrations low in the flame (because of the dominance of buoyancy in determining flame structure). As in previous studies, wire screen gulls, whose bottom edges were 22 mm above the burner surface, stabilized the flame. In addition, a cubical fine-mesh screen cage, approximately 1 m on edge, surrounded the burner assembly to isolate the flame further from laboratory air currents. The burner assembly was mounted on a two-dimensional, computer-controlled positioning system (Daedal Model 4000 controller, with a Daedal linear positioning platform mounted on a Velmax elevating table).

The Wolfhard-Parker burner system is superior to other diffusion flame burner designs for making absorption measurements. It consists of three parallel slots: a central fuel slot ($8 \text{ mm} \times 41 \text{ mm}$) and two adjacent air slots. Two symmetric flame sheets are formed at the interface of the fuel and air flow. The resulting flame shape is two dimensional, providing a relatively long (40 cm), homogeneous path length for absorption measurements. It should be noted that

because the ends of the burner are not shielded from the laboratory air, some burning does occur at the ends of the fuel slots. In the analysis of the data presented here, we have ignored these end flames. The limitations of this assumption are discussed in Appendix A.

Absorption Theory

The absorption of infrared light by a molecule in the laser beam is described by the Bouguer-Lambert law, which for a uniform line-of-sight measurement can be expressed as¹⁰

$$T_v = \left(\frac{I}{I^\circ} \right) = \exp[-Sg(v - v^\circ)P_jL]. \quad (2)$$

Here T_v is the transmissivity at frequency v , I° and I are the beam intensities before and after the absorbing sample, respectively, S is the line strength for the absorption transition, $g(v - v^\circ)$ is the line-shape factor for the wavelength dependence of the absorption (typically described assuming either a Voigt or a Lorentzian profile); P_j is the partial pressure of the absorbing species, and L is the path length. The line strength for individual P -branch lines can be calculated from the band strength collected at a reference

temperature by using

$$S_{\text{line}}(T) = S_{\text{band}}(T_{\text{ref}}) \left(\frac{T_{\text{ref}}}{T} \right) \left(\frac{E_{v',J'} - E_{v'',J''}}{E_{v',0} - E_{v'',0}} \right) \times (v'' + 1) \exp\left(\frac{-E_{v'',J''}}{kT} \right) \times \left[1 - \exp\left(-\frac{E_{v',J'} - E_{v'',J''}}{kT} \right) \right] \frac{J''}{Q_T}, \quad (3)$$

where the Q_T is the internal partition function at temperature T and the energy levels are given by

$$\frac{E_{v,J}}{hc} = \left(v + \frac{1}{2} \right) \omega_e - \left(v + \frac{1}{2} \right)^2 \omega_e x_e + J(J+1)B_e - J(J+1) \left(v + \frac{1}{2} \right) \alpha_e - [J(J+1)]^2 D_e, \quad (4)$$

where J are rotational quantum numbers, v are the vibrational quantum numbers for the two states, B_e is the rotational constant, ω_e is vibrational constant, x_e is the anharmonicity constant, α_e is the vibration-rotation interaction constant, and D_e is the centrifugal distortion constant.

A potential concern in applying high-resolution absorption measurements in atmospheric pressure combustion systems is the broadening of absorption lines. In the expression for the Voigt profile, this i^* s manifested as an increase in the dimensionless α parameter, sometimes known as the pressure-broadening parameter,¹¹ given by

$$\alpha = (\ln 2)^{0.5} \frac{\Delta\nu_C}{\Delta\nu_D}, \quad (5)$$

where $\Delta\nu_C$ and $\Delta\nu_D$ are the collision-broadened and Doppler-broadened linewidths, respectively. Hanson *et al.*¹² give expressions for both of these quantities:

$$\Delta\nu_D = 7.16 \times 10^{-7} \left(\frac{T}{M} \right)^{1/2} v_o, \quad (6)$$

$$\Delta\nu_C = 2\gamma_C (\text{cm}^{-1} \text{atm}^{-1}) \left(\frac{300}{T} \right)^n P(\text{atm}). \quad (7)$$

Here $2\gamma_C$ is the collision half-width evaluated at 300 K. For atmospheric pressure measurements at flame temperatures, the pressure-broadening parameter expected for CO is relatively large (between 2 and 3), indicative of the dominance of collisional broadening in this spectral region.

Simple kinetic theory predicts that the temperature dependence of the collision half-width n is given by $T^{-0.5}$. For pairs of molecules interacting under a Lennard-Jones 6-12 potential, Townes and Schawlow¹³ have shown that n would be expected to be $T^{-0.7}$. For CO, Hanson *et al.*¹² found that the temperature dependence of the collisional linewidth was on average given by $n = 0.67$ in premixed flame

systems. In subsequent research Varghese and Hanson¹⁴ showed that n depended on both the rotational state of the absorbing species and the temperature range; i.e., a different value of n was needed for low temperatures than at higher temperatures. In studies in premixed methane-air flames, these authors were able to predict the overall collision widths for CO by estimating the contribution from individual colliders in the combustion mixture.

It has been demonstrated that the sensitivity of tunable diode-laser measurements can be increased by modulating the laser wavelength.¹⁵ If the modulation frequency is large with respect to the feature width (also expressed in frequency), then the technique is known as frequency modulation spectroscopy. The inverse case (relatively low modulation frequencies) is known as wavelength modulation spectroscopy. Wavelength modulation spectroscopy may improve sensitivities 3 orders of magnitude over conventional absorption detection.¹⁵ Frequency modulation extends sensitivities even further, perhaps another 3 orders of magnitude.¹⁶

For weak absorptions,

$$\ln\left(\frac{I^\circ}{I} \right) = \ln\left[\frac{I^\circ}{(I^\circ - x)} \right] \approx \frac{x}{I^\circ}, \quad (8)$$

where x is the intensity of the absorption signal. This approximation is appropriate when there is less than $\approx 5\%$ absorption of the incident radiation.

In modulation spectroscopy an oscillation is applied to the diode-injection current as the laser is being scanned through an absorption feature. If the signal is sampled at the modulation frequency, the resulting signal profile has an appearance similar to the first derivative of the detector intensity; if the signal is sampled at twice the modulation frequency (known as $2f$ detection), the processed signal looks like the second derivative, and so on. The magnitude of the second-harmonic signal x'' is a function of the direct absorption signal.¹⁷ For weak absorptions,

$$x'' = H_2(v - v_o) Sg(v - v_o) P_j L I^\circ, \quad (9)$$

where $H_2(v - v_o)$ is the second Fourier coefficient of the time-dependent absorption coefficient.¹⁵ The amplitude of the modulation will obviously determine the magnitude of the harmonic signal. Arndt¹⁷ showed that the maximum center-line second-harmonic signal, i.e., the maximum value of $H_2(0)$, will be observed when the normalized modulation amplitude (defined as the modulation amplitude divided by the absorption half-width) is equal to 2.2 for Lorentzian lines. In that case, $H_2(0)$ equals 0.343.

Steep temperature gradients exist in diffusion flames, and therefore linewidths will vary with spatial location. If the modulation amplitude is fixed, $H_2(0)$ will vary with location in the flame. An alternative approach to the quantitative application of wavelength-modulation spectroscopy would be to calibrate the signal either directly, by observing signal strengths

for known concentrations,¹⁸ or against a direct absorption signal and then correct for the variation in the local linewidth. The latter is the approach adopted here.

Studies of Carbon Monoxide

Fitting Lines: Voigt versus Lorentzian

As we noted above, the expected Voigt pressure-broadening parameter for CO is close to three for our flame conditions. This value is sufficiently high that it may not be necessary to fit spectral lines by using Voigt line shapes, but rather by using a computationally simpler Lorentzian line shape. Figure 2 shows absorption-data for the $P(8)$ rotational line of CO at a height of 9 mm above the burner surface and -4 mm from the plane of symmetry running through the center of the burner. A three-parameter Lorentzian line shape fit was made to the data, with the independent parameters being the partial pressure of CO, the baseline level, and the room-temperature collision half-width. The baseline level tracks nonresonant effects, which might include extinction caused by particles and beam steering by the flame's temperature gradients. The half-width at flame temperatures is calculated from the room-temperature value by assuming a $T^{-0.67}$ dependence.¹³ The tempera-

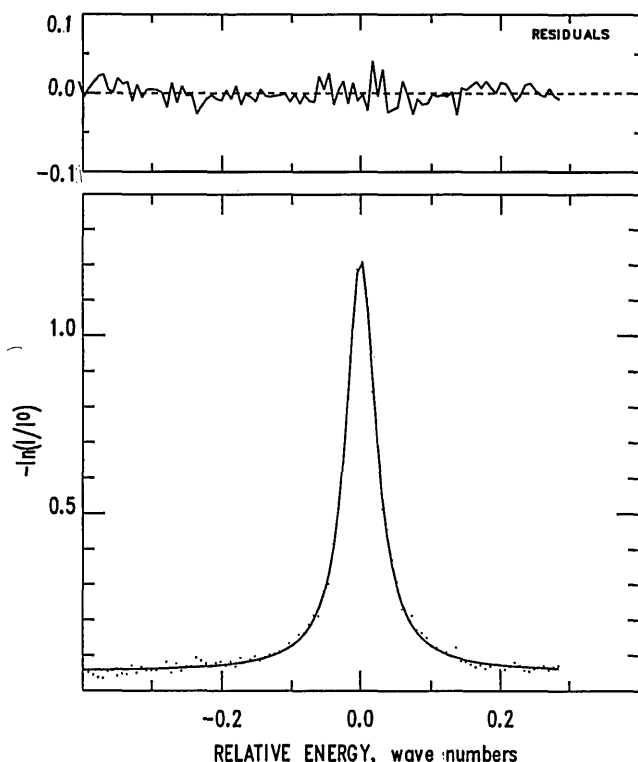


Fig. 2. Fit of the CO $P(8)$ transition using a Lorentzian line-shape function. The spectrum was recorded at $+3.0$ mm from the center of the burner at a height of 9 mm above the burner's surface. The temperature, determined from a prior thermocouple measurement,⁶ was 1157 K. The abscissa for these plots is the digital-to-analog converter count index for the current control module. The entire spectrum (1500 counts) corresponds to roughly 0.75 cm^{-1} .

ture used in the fit was that determined for this flame system previously using Pt-Pt/Rh thermocouples.⁷

As we can see from a comparison of the fit to the data, the Lorentzian function adequately describes the experimental line shape with no systematic errors apparent in the trace of the residual profile. We have also done fits of the data to a Voigt line-shape function. These fits took considerably more computation time for convergence and produced no more satisfactory appearing agreement with the experimental data. Therefore, only Lorentzian fits were used for the CO concentration profile measurements to be described below.

Profile Measurements

Transmission traces for five different rotational lines of CO [$P(8)$, $P(11)$, $P(12)$, $R(2)$, and $R(11)$] were collected every 0.2 mm from -8 mm to $+8$ mm and every 0.5 mm from 8 to 10 mm (relative to the burner center) at a height of 9 mm above the burner surface. These spectra were fit by using the three-parameter Lorentzian line-shape analysis described above. The results of these fits showed that the collision half-width showed a monotonic decrease from approximately 5 mm in toward the center of the flame, with an overall decrease of approximately $0.015 \text{ cm}^{-1} \text{ atm}^{-1}$. The upper limit (near ± 5 mm) was generally higher for low J'' states ($\approx 0.09 \text{ cm}^{-1} \text{ atm}^{-1}$ for $J'' = 2$) and lower for high J'' states ($\approx 0.065 \text{ cm}^{-1} \text{ atm}^{-1}$ for $J'' = 12$). Outside of ± 5 mm, CO concentrations decreased rapidly as a result of oxidation, and the fits' half-widths and CO partial pressures became more random. Near the high-temperature reaction zone of this flame (which occurs at ± 6.6 mm at this height) the major species, determined by quartz microprobe-mass spectrometric measurements, are N_2 (≈ 70 mol. %), H_2O (≈ 20 mol. %), and CO_2 (≈ 10 mol. %).⁷ From this location outward the N_2 rises to near its ambient air value and the CO_2 and H_2O are replaced by O_2 . To determine CO concentrations more accurately as the reaction zone is approached, we have used the measured mole fractions of N_2 , O_2 , H_2 , H_2O , CO , CH_4 , and H_2 (Ref. 7) combined with their collision half-widths with CO (Refs. 14 and 19) to calculate the overall collision half-width for CO absorption lines as a function of flame position. The CO spectra were then refit by using a two-parameter fit with these calculated half-widths. Near the center of the flame, where fits both with and without half-width as an adjustable parameter could be performed, relatively little difference was observed between the resulting concentrations. For example, the three-parameter fit at lateral position 0.0 gave 8.7 mol. % for the concentration of CO, whereas the two-parameter fit gave 7.1 mol. %. The differences between the two fits decreased as the position from the burner's center was increased. It should be noted that at the center of the flame the mixture is dominated by methane, whose CO collision half-width was *not* determined by Varghese and Hanson.¹⁴ Because of low absorption levels, the concentra-

tions of CO at the lean edges of the flame (position greater than ≈ 6.5 mm from the burner center line) are unreliable with the direct-absorption technique. For flame locations outside of ± 6.5 mm we established the CO concentration by the direct-absorption technique and used that to calibrate a second-harmonic signal at the same spatial location. Concentrations for other spatial locations were calculated by ratioing the second-harmonic signals to that of the calibration point and then correcting for local line strengths and line-shape factors, both of which are known functions of temperature. The overall collision half-widths calculated from the local flame mixture were used in the calculation of the line-shape factor.

Figure 3 shows the concentration profile calculated from $P(8)$ direct-absorption spectra and $P(11)$ wavelength-modulation spectra at a height of 9 mm above the burner surface. Data from -6 mm to 6 mm were from the direct-absorption fits. Concentrations outside of ± 6 mm were from wavelength-modulation measurements. Also shown is a profile determined from quartz microprobe-mass spectrometer measurements and a relative profile of CO mole fraction determined from the laser-induced fluorescence measurement.⁵ For the latter profile, the following procedure was followed to extract relative CO concentrations. Laser-induced fluorescence (LIF) was observed for the vibronic bands of the $B^1\Sigma^+ \rightarrow A1\pi$ transition following two-photon excitation of the $X^1\Sigma^+ \rightarrow B^1\Sigma^+(0,0)$ transition. Profiles were obtained with the laser tuned on and resonance at the Q branch head,

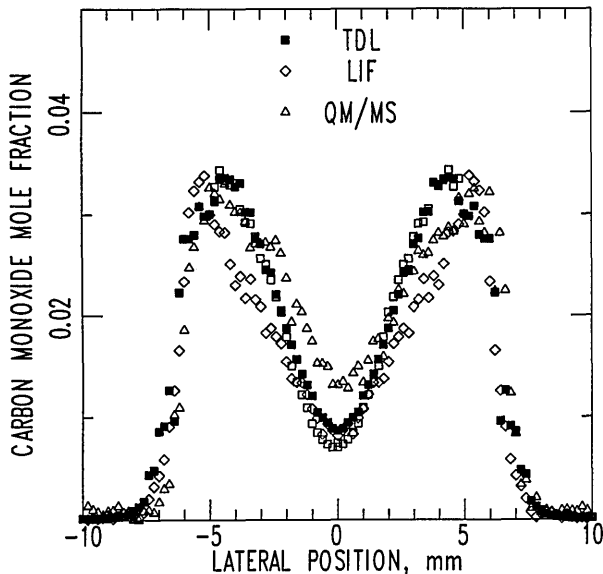


Fig. 3. Profile of CO concentration determined from a series of $P(8)$ direct-absorption spectra and $P(11)$ second-harmonic spectra. The solid squares are concentrations from fits of spectral data in which the collision half-width was calculated from the local composition of the flame. The open squares were fits of spectra data in which the half-width was an adjustable parameter of the fit. These data are compared with profiles of CO determined from LIF (diamonds) and quartz microprobe-mass spectrometer (QM/MS) measurements (triangles).

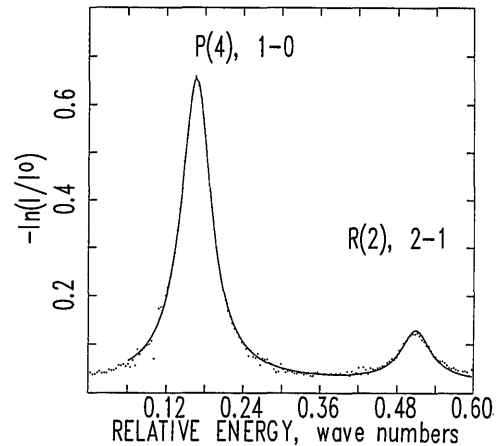


Fig. 4. Simultaneous fits of the CO $P(4)$ ($1 \leftarrow 0$, 2127.68 cm^{-1}) and $R(2)$ ($2 \leftarrow 1$, 2128.01 cm^{-1}) lines at 9 mm HAB and 3 mm from the burner center line.

then net LIF profiles were derived. There is no quenching correction needed; the experiments were done under conditions in which ionization from $B^1\Sigma^+$ was much greater than the quenching rate. There was a major correction necessary to account for how Q -branch head intensity varied with temperature, i.e., how many rotational levels were excited by the laser at the local flame temperature.²⁰ Finally, the peak concentration for CO was assumed to be the same as that found in the TDL measurements: 3.4 mol. %. This concentration shows good agreement among the three measurements.

Temperature Measurements

It has been demonstrated that absorption across two spectrally adjacent CO rotational lines that originate in different vibrational levels can be used to determine the flame temperature.^{21,22} Figure 4 shows simultaneous fits of the CO $P(4)$ ($1 \leftarrow 0$, 2127.68 cm^{-1}) and $R(2)$ ($2 \leftarrow 1$, 2128.01 cm^{-1}) lines at 9-mm height above burner and -3.8 mm from the burner

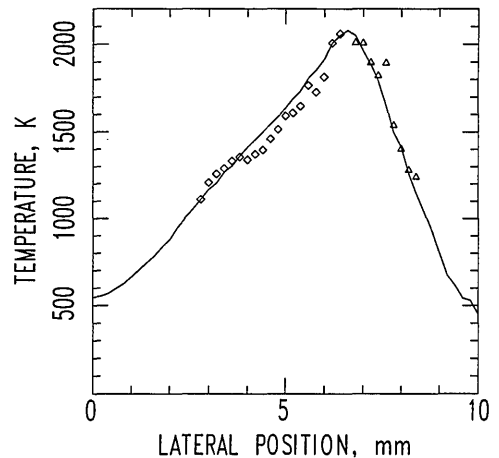


Fig. 5. Comparison of the temperature profile at 9 mm HAB determined from radiation-corrected thermocouple measurements (solid curve), direct-absorption TDL (diamonds) and second-harmonic TDL (triangles).

center line. For this calculation, it was assumed that both lines had the same room-temperature collision half-width. Thermocouple measurements gave 1367 K for the temperature at this flame location (after a radiation correction had been applied, see Ref. 7, which is in excellent agreement with the temperature from the fit of this data: 1356 K.

Figure 5 compares a profile of the TDL temperature measurements with that of the thermocouple measurements. As was true for the concentration measurements, direct-absorption signal levels were low at the lean edges of the flame, and reliable fitting of the experimental data was not possible. For these flame regions the ratio of the center-line second-

harmonic signals will be the same as the ratio of the two line strengths, which is a known function of temperature.²¹ As the data in Fig. 5 indicate, TDL absorption provides a reasonably accurate measurement of temperature in this flame system: we estimate the direct-absorption measurements to provide accuracy of ± 100 K and the center-line harmonic signal measurements to be good to ± 200 K. Moreover, the shape of the temperature profile is nearly identical for the TDL and thermocouple techniques. Improved accuracy might be possible by selecting CO line pairs that exhibited a greater dependence of line-strength ratio on temperature.^{21,22}

Conclusion

We have demonstrated the application of TDL's to *in situ* diagnostics in laminar hydrocarbon diffusion flames. For the methane-air flame described here, the results for both CO concentration and local flame temperature are in excellent agreement with prior measurements of these quantities that use probe and optical techniques.

Appendix A: Interference of End Flames in Absorption Measurements

As we noted above, in our Wolfhard-Parker design, end flames burning at the edge of the fuel slot may interfere with absorption measurements. To investigate the magnitude of the error introduced by assuming a perfectly homogeneous absorption path, we have modeled absorption profiles with and without end flames. It has been noted for some years that the concentrations of many species and temperature in laminar hydrocarbon diffusion flames correlate with mixture fraction, or alternatively, local equivalence ratio.^{2,7,23,24} Furthermore, for major species these correlations are relatively independent of geometry. Therefore, once the spatial profile for the mixture fraction has been established, it is possible to approximate both these species' concentrations and the local temperature. We have used our Wolfhard-Parker database to calculate the mixture fraction as a function of lateral position 9 mm above the burner surface and to correlate the observed CO concentration to it. The expected concentration of CO was mapped onto the ends of the burner system by using this mixture-fraction correlation with stoichiometric burning assumed to occur directly above the ends of the fuel slot. The same procedure was followed for the local flame temperature. Figure 6 shows the expected CO concentration and temperature profiles at 9 mm above the burner surface using this procedure.

A program was then written to calculate the extinction of laser light along a beam parallel to the burner slots at v^0 for various CO transitions assuming either the presence or absence of these end flames. Figure 7 compares these results for the two lines used in the temperature measurements described above. This calculation shows that from approximately 3 mm from the burner plane of symmetry and outward, the

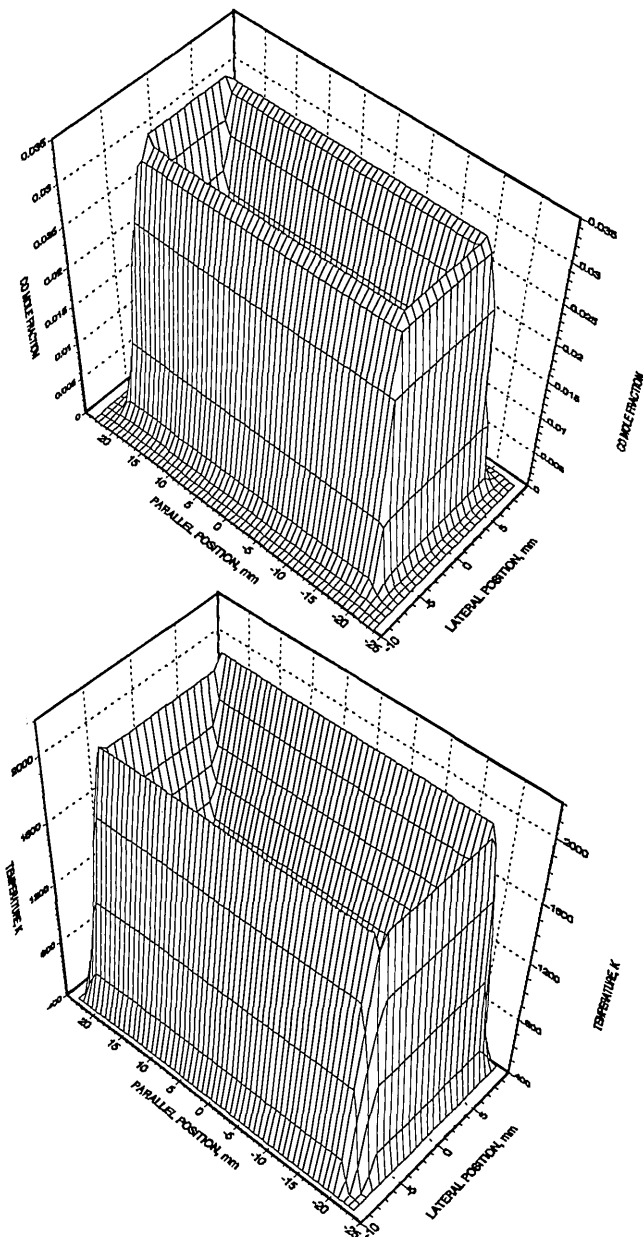


Fig. 6. Calculated CO and temperature profiles at 9 mm above the burner surface, illustrating location of end flames. The label LATERAL POSITION refers to the direction perpendicular to the fuel and air slots.

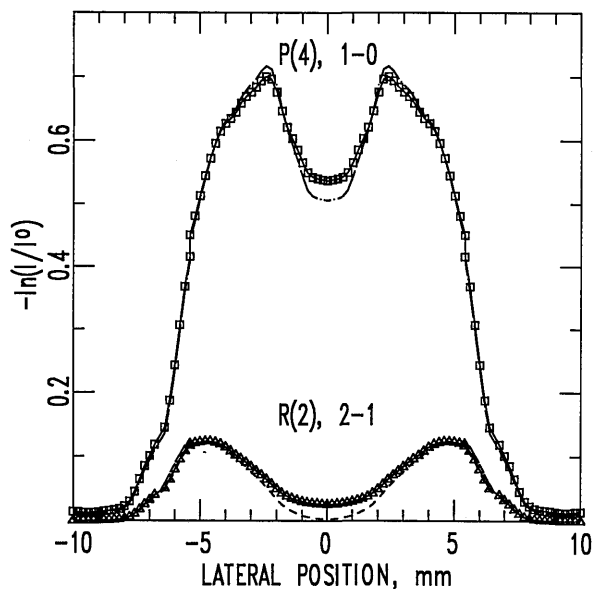


Fig. 7. Calculated absorbances at line center for the $P(4) 1 \leftarrow 0$ and $R(2) 2 \leftarrow 1$ lines. In each case the trace with symbols is the extinction for a flame with end flames. The trace without symbols is the calculated extinction for a flame without end flames.

end flames have little impact on the extinction of laser light by CO. However, for both lines the end flames increase the extinction near the center of the burner. This increase is relatively greater for lines that have high initial energies; i.e., either large J'' and $v'' = 0$ or any rotational members of $v'' > 0$. The implication of these results is that the most accurate concentration measurements of CO near the flame center will be favored by absorption from $v'' = 0$, low J'' . However, because calculated temperatures are functions of the ratio of the absorbances of lines originating in different v'' levels, temperatures calculated near the burner center would be dramatically in error.

This work was supported by the National Science Foundation under grant NSF-CTS-8906472 and the National Institute of Standards and Technology under grant DOC 60NANB9DO963.

References

1. R. A. Yetter, F. L. Dryer, and H. Rabitz, "Complications of one-step kinetics for moist CO oxidation," in *Twenty-First Symposium (International) on Combustion* (Combustion Institute, Pittsburgh, Pa., 1986), pp. 749–760.
2. R. E. Mitchell, A. F. Sarofim, and L. A. Clomburg, "Experimental and numerical investigation confined laminar diffusion flames," *Combust. Flame* **37**, 227–244 (1980).
3. W. M. Pitts, "A long range plan for a research project on carbon monoxide production and prediction," *Natl. Inst. Stand. Technol. Int. Rep.* **89-4185** (1989).
4. K. Brezinsky, "High temperature oxidation of aromatic hydrocarbons," *Prog. Energy Combust. Sci.* **12**, 1–24 (1986).
5. P. J. H. Tjossem and K. C. Smyth, "Multiphoton excitation spectroscopy of the $B^1\Sigma^+$ and $C^1\Sigma^+$ Rydberg States of CO," *J. Chem. Phys.* **91**, 2041–2048 (1989).
6. A. Hamins and J. H. Miller, George Washington University, Washington, D.C. 20052 (personal communication, 1989).
7. K. C. Smyth, J. H. Miller, R. C. Dorfman, W. G. Mallard, and R. J. Santoro, "Soot inception in a methane/air diffusion flame as characterized by detailed species profiles," *Combust. Flame* **62**, 157–181 (1985).
8. R. J. Santoro, Pennsylvania State University, University Park, Pa. 16801 (personal communication, 1989).
9. K. C. Smyth, P. J. H. Tjossem, A. Hamins, and J. H. Miller, "Concentration measurements of OH and equilibrium analysis," *Combust. Flame* **79**, 366–380 (1990).
10. G. Guelachvili and K. Rao, *Handbook of Infrared Standards* (Academic, Orlando, Fla., 1986).
11. S. M. Schoenung and R. K. Hanson, "Laser absorption sampling probes for temporally and spatially resolved combustion measurements," *Appl. Optics* **21**, 1767–1771 (1981).
12. R. K. Hanson, P. L. Varghese, S. M. Schoenung, and P. K. Falcone, "Absorption spectroscopy of combustion gases using a tunable IR diode laser," in *Laser Probes for Combustion Chemistry*, No. 134 of ACS Symposium Series (American Chemical Society, Washington, D.C., 1980), pp. 413–426.
13. C. H. Townes and A. L. Schawlow, *Microwave Spectroscopy* (Dover, New York, 1975).
14. P. L. Varghese and R. K. Hanson, "Tunable infrared diode laser measurements of line strengths and collision widths of $^{12}\text{C}^{16}\text{O}$ at room temperature," *J. Quant. Spectrosc. Radiat. Transfer* **26**, 339–347 (1981).
15. J. Reid and D. Labrie, "Second harmonic detection with tunable diode lasers—comparison of experiment and theory," *Appl. Phys. B* **26**, 203–210 (1981).
16. J. Silver, "Frequency modulation spectroscopy for trace species detection: theory and comparison among experimental methods," *Appl. Opt.* **31**, 707–717 (1992).
17. R. Arndt, "Analytical line shapes for Lorentzian signals broadened by modulation," *J. Appl. Phys.* **36**, 2522–2524 (1965).
18. J. A. Silver, D. S. Bomse, and A. C. Stanton, "Diode laser measurements of trace concentrations of ammonia in an entrained flow coal reactor," *Appl. Opt.* **30**, 1505–1511 (1991).
19. G. T. T. Tejwani and P. Varanasi, "Calculation of collisionally broadened linewidths in the infrared bands of methane," *J. Chem. Phys.* **55**, 1075–1083 (1971).
20. K. C. Smyth, National Institute of Standards and Technology, Gaithersburg, Md. 20838 (personal communication, 1990).
21. R. K. Hanson and P. K. Falcone, "Temperature measurement technique for high-temperature gases using a tunable diode laser," *Appl. Opt.* **17**, 2477–2480 (1978).
22. X. Ouyang and P. L. Varghese, "Selection of spectral lines for combustion diagnostics," *Appl. Opt.* **29**, 4884–4890 (1990).
23. R. W. Bilger, "Reaction rates in diffusion flames," *Combust. Flame* **30**, 277–284 (1977).
24. R. W. Bilger, "Turbulent diffusion flames," *Annu. Rev. Fluid Mech.* **21**, 101–135 (1989).